

Non-Ideality of a DNA Strand Displacement AND Gate Studied with a Dynamic Bonded DNA Model

Carsten Svaneborg · Harold Fellermann · Steen Rasmussen

Received: date / Accepted: date

Abstract We perform a spatially resolved simulation study of an AND gate based on DNA strand displacement using several lengths of the toehold and the adjacent domains. DNA strands are modelled using a coarse-grained dynamic bonding model [C. Svaneborg, *Comp. Phys. Comm.* 183, 1793 (2012)]. We observe a complex transition path from the initial state to the final state of the AND gate. This path is strongly influenced by non-ideal effects due to transient bubbles revealing undesired toeholds and thermal melting of whole strands. We have also characterised the bound and unbound kinetics of single strands and in particular the kinetics of the total AND operation and the three distinct DNA transitions that it is based on. We observe an exponential kinetic dependence on the toehold length of the competitive displacement operation, but that the gate operation time is only weakly dependent on both the toehold and adjacent domain length. Our gate displays excellent logical fidelity in three input states, and quite poor fidelity in the fourth input state. This illustrates how non-ideality can have very selective effects on fidelity. Simulations and detailed analysis such as those presented here provide molecular insights into strand displacement computation, that can also be expected in chemical implementations.

Keywords computer simulation · DNA strand displacement computation · gate fidelity · gate kinetics · physical simulation

C. Svaneborg · H. Fellermann · S. Rasmussen
Centre for Fundamental Living Technology, Department of Physics, Chemistry and Pharmacy,
University of Southern Denmark, Campusvej 55, DK-5320 Odense, Denmark, E-mail:
science@zqex.dk, E-mail: harold@sdu.dk, and E-mail: steen@sdu.dk

H. Fellermann
Complex Systems Lab, Barcelona Biomedical Research Park, Universitat Pompeu Fabra, Dr.
Aiguadé 88, 08003 Barcelona, Spain,

S. Rasmussen
Santa Fe Institute, 1399 Hyde Park Road, Santa Fe NM 87501, USA

1 Introduction

Ever since the pioneering work of Adleman in 1994 (Adleman 1994), DNA has been recognized as a massively parallel, versatile, and inexpensive computing substrate. In order for such substrate to be of practical interest, however, it is desirable that the computational framework is scalable and that individual computational elements can be combined to form more complex circuits. Recently, a scalable approach to enzyme-free DNA computing has been proposed where logic gates consist of relatively short DNA strands that communicate via strand displacement (Seelig et al 2006; Qian and Winfree 2011). Strand displacement is also used to control the communication between DNA decorated chemical containers (Hadorn and Eggenberger Hotz 2010; Hadorn et al 2012; Gil et al 2013; Amos et al 2011).

In the strand displacement approach to DNA computation, individual gates consist of one DNA template that is composed of several logical domains. In their initial state, all domains but one are hybridized to one or more complementary strands and are therefore inert. The only exposed single strand domain of each gate is a short toehold region at one end of the template. This toehold region can reversibly bind a complementary signal strand which is designed to be longer than the toehold domain and complementary to the next domain(s) of the template. The newly binding signal is then able to hybridize to all matching domains of the template, thereby displacing strands that were previously bound and possibly exposing new toeholds (Zhang and Winfree 2009). The displaced strands can be fluorescent output signals, or internal signals that can bind to toehold regions of downstream gates. Ideally, by choosing domains and toeholds of appropriate length, toehold binding will be reversible whereas the total strand displacement process is irreversible. Hence computation is energetically downhill and kinetically irreversible, if and only if the correct input strands are present and match the logical setup of the gates. It has been shown that this approach leads to modular logic gates that enable the design of large scale DNA circuits (Cardelli 2011; Lakin et al 2012).

Despite the fact that DNA self-assembly and strand-displacement operations are widely utilized in the field of DNA nanotechnology, only little is known about their kinetics (Zhang and Winfree 2009). In the present paper, we study effects of non-ideality on the kinetics and fidelity of a strand displacement AND gate using a spatially resolved coarse-grained DNA model. (Svaneborg 2012) Fig. 1 shows the AND gate design that we are simulating. It consists of two toeholds of identical length t and two adjacent domains of identical length l . Note that we do not presently worry about garbage collecting the blocking strand after it has been displaced (Cardelli 2011).

When DNA computation is implemented in terms of real molecular reactions we have to content with non-ideality. The most important source of non-ideality is that experiments are carried out at non-zero temperature. The probability of a given molecular DNA state is not just determined by the binding energy (as at absolute zero temperature), but by the free energy which also contains entropic contributions. The most likely molecular state is that which has a minimal free energy, which is a temperature dependent balance between minimizing the energy and maximizing the entropy. At finite temperatures, stretches of DNA nucleotides will spontaneously dehybridize, such that the resulting bubbles increase the configurational entropy and hence reduce the free energy of the double strand (Altan-Bonnet et al 2003; Blossey and Carlon 2003; Jost and Everaers 2009). As the temperature is increased towards the melting temperature (where half of the hybridization bonds are present on average), these bubbles grow in

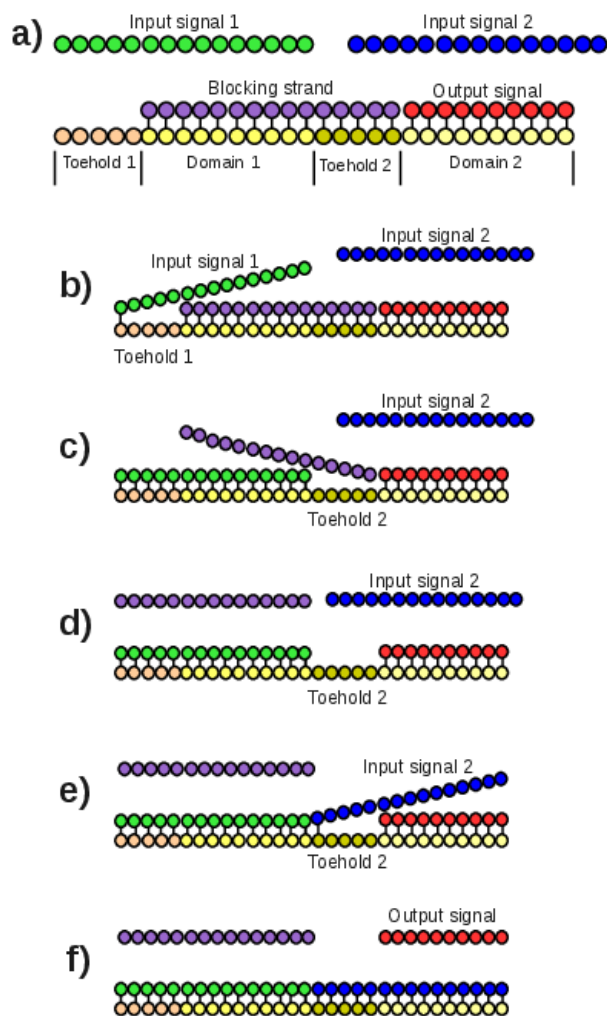


Fig. 1 Design of the AND gate using a template with two toeholds and domains. Ideally the gate operates as follows: a) initially toehold 1 is exposed, a blocking strand (magenta) protects toehold 2, and the output signal strand (red) is hybridized with domain 2. b) Signal strand 1 (green) hybridizes with toehold 1 and c) reversibly displaces the blocking strand whereby d) toehold 2 is freed. e) Signal strand 2 (blue) hybridizes with toehold 2 and f) irreversibly displaces the output signal strand (red).

size until the double strand thermally melts forming two free strands. Bubbles are more likely to be found at the end of a double stranded domain, as these are less stable due to the lacking stacking interaction at the end (SantaLucia and Hicks 2004). When two neighbouring strands are hybridized to a template, a single backbone bond is also missing at the interface between them. And this nick is also less stable (Lane et al 1997; Protozanova et al 2004). These effects of non-ideality affect DNA strand computation operation since bubbles transiently expose nucleotides and hence enables undesired strand displacement operations to take place. Thermal melting can also release strands that were expected to be irreversible bound to the template. Transient states along pathway from an initial to a final states can also have a higher free energy. In this case, the transition state with the highest free energy along the pathway will determine the transition rate and it will depend exponentially on the height of the free energy barrier relative to the initial state (Kramers 1940). For instance, it has been observed that strand displacement slows down exponentially as the toeholds become longer. (Yurke and Mills 2003).

The chemical structure of short DNA oligomers can be studied with atomistic molecular dynamics simulations such as Amber (Case et al 2010; Cheatham III and Young 2000) and Charmm (Brooks et al 2009; MacKerell Jr et al 2000). However, if we are only interested in secondary structure, it is more effective to utilize coarse-grained simulation models. Coarse-graining is a statistical physical technique by which irrelevant microscopic details are systematically removed, producing an effective model (Langowski 2006; de Pablo 2011) with the same mesoscopic properties. The major computational advantage of coarse-graining is that it allows us to focus our computational resources on studying the mesoscopic DNA structures and dynamics of interest.

Coarse-grained models describe a nucleotide by a small number of effective interaction sites. In the “three sites per nucleotide” model of de Pablo and co-workers, three sites represent the phosphate backbone site, the sugar group, and the base, respectively (Sambriski et al 2009b,a). There is also a number of “two sites per nucleotide” models, e.g. the model of Ouldrige and co-workers (Ouldrige et al 2010, 2011), where one site represents the base and another site the backbone and the sugar ring. Savelyev and Papoian (Savelyev and Papoian 2010) have formulated a “one site per nucleotide” model. As the number of interaction sites per nucleotide is reduced, the chemical structure is progressively lost. In simulations of DNA tagged nano-particles, even more coarse-grained models are used. DNA molecules have been modelled e.g. as semi-flexible polymers with attractive sites on each monomer (Hsu et al 2010), or as a single sticky site that can be hybridized with free complementary free sticky sites (Martinez-Veracoechea et al 2011). While the chemical structure of DNA has been completely eliminated, these models still retain the DNA sequence specific hybridization effects on nano-particle self-assembly.

We are interested in studying the statistical mechanics of hybridizing DNA strands and in particular the kinetics of DNA self-assembly and DNA computation using a DNA model that is as coarse-grained as possible. We have implemented a general framework that allows for directional bonds to be reversibly formed and broken during molecular dynamics simulations (Svaneborg 2012). Along with the bonds, the angular and dihedral interactions required to model the residual effects of chemical structure are also dynamically introduced and removed as dictated by the bond dynamics. This framework allows us to simulate reversible hybridization of complementary beads and chains built from such beads. In the present paper, we study a minimal dynamic bonding DNA model. For simplicity, we assume that the binding energy, as well as

the bond, angular, and dihedral potentials are independent of sequence, and we have chosen a force field that produces a flat ladder-like structure in the double stranded state. Our motivation for these choices is to minimize the number of required model parameters.

Dynamic bonding DNA models combine ideas from most of the existing DNA models. We regard them as dynamic generalizations of statistical mechanical theories and simultaneously as simplifications of coarse-grained DNA models. As in the Poland-Scheraga model of DNA melting (Poland and Scheraga 1966; Jost and Everaers 2009), complementary base pairs can either be hybridized or open. When a base pair is hybridized, it is characterized by a continuous hybridization potential as in the Dauxois-Peyrard-Bishop model (Peyrard et al 2008). Dynamic bonding DNA models can also be regarded as off-lattice generalizations of the lattice Poland-Scheraga model (Jost and Everaers 2007). Rather than trying to model chemical structure with interaction sites as in the “two and three sites per nucleotide” models (Sambriski et al 2009b,a; Ouldrige et al 2010, 2011) dynamic bonding DNA models use angular and dihedral interactions to model the residual effects of local chemical structure. Dynamic bonded DNA double stands can reversibly melt and re-anneal, which is not possible with the “one site per nucleotide model” of Savelyev and Papoian (Savelyev and Papoian 2010) due to the special “fan” interactions it uses between stretches of opposing nucleotides. Finally, as in the sticky DNA models (Martinez-Veracochea et al 2011), a single bead in a dynamic bonding DNA model can equally well represent a domain.

Sect. 2 introduces the dynamic bonding DNA model. We present the simulation results and discussion in Sect. 3 and a conclusion in Sect. 4.

2 Model

In the present dynamic bonding DNA model, single stranded DNA (ssDNA) is represented by a string of nucleotide beads connected by stiff springs representing directional backbone bonds. Complementary beads can reversibly form hybridization bonds. Rather than limiting the model to represent the ACGT nucleotides, we increase the alphabet maximally to avoid getting trapped in misaligned transient hybridization states. A novel feature of our DNA model is that it involves dynamic hybridization bonds, which are introduced or removed between complementary interaction sites or beads when they enter or exit the hybridization reaction radius. Along with the bonds, we dynamically introduce or remove angular and dihedral interactions in the chemical neighbourhood of a hybridizing bead pair. These interactions are introduced based on the local bond and bead type pattern, and hence allows us to retain some effects of the local chemical structure in coarse-grained models. We utilize bonds carrying directionality to represent the 3'-5' backbone structure of DNA molecules. This allows us to introduce dihedral interactions that can distinguish between parallel and anti-parallel strand alignments. We have implemented this framework in a modified version of the Large-scale Atomic/Molecular Massively Parallel Simulator (LAMMPS) (Plimpton 1995; Svaneborg 2012).

The DNA model relies on two ingredients, a Langevin dynamic for propagating a system in time and space, and a dynamic directional bonding scheme (Svaneborg 2012) that propagates the chemical structure of the system. The force on bead i is given by a Langevin equation

$$\mathbf{F}_i = -\nabla_{\mathbf{R}_i} U - \frac{m}{\Gamma} \dot{\mathbf{R}}_i + \boldsymbol{\xi}_i \quad \text{with} \quad U = U_{\text{bond}} + U_{\text{angle}} + U_{\text{dihedral}} + U_{\text{pair}}.$$

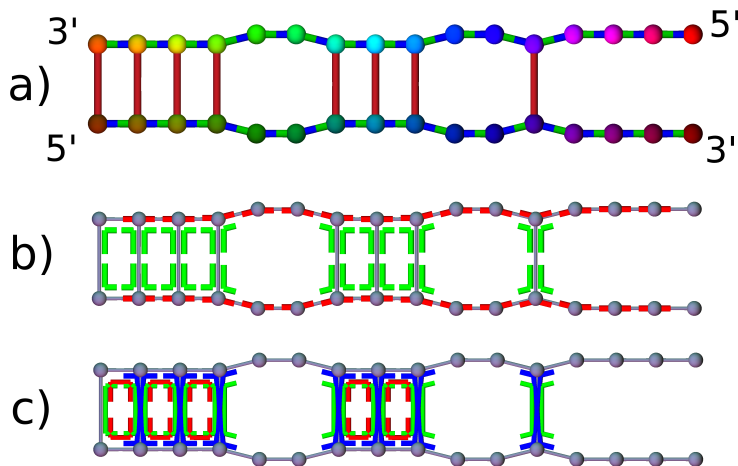


Fig. 2 Illustrative DNA conformation with partial hybridization. a) nucleotide beads (different hues indicate complementarity), backbone bonds (green-blue indicates 3'-5' bond direction), and hybridization bonds (red); b) angular interactions indicated by lines parallel to the two bonds involved (red/green colours indicate the type of interaction); c) dihedral interactions indicated by lines parallel to the three involved bonds (red/green/blue colours indicate the type of interaction). The figure is explained in the text.

Here, the first term denotes a conservative force derived from the potential U . The second term is a velocity dependent friction, and the third a stochastic driving force characterized by $\langle \xi_i(t) \rangle = 0$ and $\langle \xi_i(t) \xi_j(t') \rangle = k_B T m / (\Gamma \Delta t) \delta_{ij} \delta(t - t')$. The potential U comprises four terms representing bond, angular, dihedral, and non-bonded pair interactions, respectively. The friction and stochastic driving force implicitly represents the effect of a solvent with a specified friction and temperature. The Langevin dynamics is integrated using a Velocity Verlet algorithm with a time step $\Delta t = 0.001 \tau_L$ and $\Gamma = 2 \tau_L$ using a customized version of LAMMPS (Plimpton 1995; Svaneborg 2012).

Here and in the rest of the paper we use reduced units defined by the Langevin dynamics and DNA model. The unit of energy is $\epsilon = k_B T$, where we set Boltzmann's constant k_B to unity. The bead-to-bead distance along a single strand defines the unit of length σ . The mass is $m = 1$ for all beads. A Langevin unit of time is defined as $\tau_L = \sigma \sqrt{m/\epsilon}$.

Fig. 2a shows complementary nucleotide beads with the same hue but different levels of colour saturation. As a simplification, we allow each bead only to hybridize with a single complementary bead. The DNA model has two types of bond interactions: permanent backbone bonds (shown green/blue) and dynamic hybridization bonds (shown red). Backbone bonds (subscript bb) and hybridization bonds (subscript hyb) are characterized by the two potentials:

$$U_{\text{bond,bb}}(r) = \frac{U_{\text{min,bb}}}{(r_c^{\text{b}} - r_0^{\text{b}})^2} \left((r - r_0^{\text{b}})^2 - (r_c^{\text{b}} - r_0^{\text{b}})^2 \right),$$

and

$$U_{\text{bond,hyb}}(r) = \begin{cases} \frac{U_{\text{min,hyb}}}{(r_c^{\text{h}} - r_0^{\text{h}})^2} \left((r - r_0^{\text{h}})^2 - (r_c^{\text{h}} - r_0^{\text{h}})^2 \right) & \text{for } r < r_c^{\text{h}} \\ 0 & \text{for } r \geq r_c^{\text{h}}. \end{cases}$$

In the simulations, we use $U_{\min,bb} = 100\epsilon$, $r_0^b \equiv 1\sigma$, and $r_c^b = 1.2\sigma$, $r_0^h = 2\sigma$ and $r_c^h = 2.2\sigma$. Note that $U_{\text{bond,hyb}}(r) \leq 0$ for all distances. When two non-hybridized beads of complementary type are within a reaction distance r_c^h a hybridization bond is introduced between them. If they move further apart than r_c^h again, the hybridization bond is broken. The pair-interaction between all beads is given by a soft repulsive potential, while we use the same potential function for angular and dihedral interactions. They are given by

$$U_{\text{pair}}(r) = A \left[1 + \cos\left(\frac{\pi r}{r_c^p}\right) \right] \quad \text{for } r < r_c^p,$$

where we use $A = 1\epsilon$ and $r_c^p = 1\sigma$ in the simulations, and

$$U(\Theta; \Theta_0, U_{\min}) = -\frac{U_{\min}}{2} (\cos[\Theta - \Theta_0] + 1),$$

Along the backbone of single strands we use a permanent angular interaction defined by $U(\Theta; \Theta_0 = \pi, U_{\min} = 25\epsilon)$. This determines the persistence length of single strands. In Fig. 2b backbone angular interactions are shown as thick red lines around the central bead defining the angle.

In real DNA molecules, the hydrogen bonds between Watson-Crick complementary nucleotides act together with stacking interactions and the phosphodiester backbone bonds to give rise to a helical equilibrium structure of the double strand. In our coarse-grained model, we utilize angular and dihedral interactions to determine the ladder-like equilibrium structure of our DNA model and to control the collective zipper dynamics. To control the stiffness of the double strands and to ensure anti-parallel 3'-5' alignment of the two single strands, we have assigned directionality to the backbone bonds (Svaneborg 2012). This is also necessitated by the fact that the 3' and 5' carbons of the nucleotide sugar ring have been merged into one single nucleotide bead. Fig. 2a shows the backbone bonds coloured green/blue to indicate the 3' and 5' ends, respectively.

When a hybridization bond is introduced, we also dynamically add angular interactions between the hybridization bond and the neighbouring backbone bonds. These angular interactions are characterized by the potential $U(\Theta; \Theta_0 = \pi/2, U_{\min,a})$, which favours a right angle conformation. When a hybridization bond is broken, concomitantly all the associated angular interactions are removed. In Fig. 2b the angular interactions are shown as green lines indicating the angle.

Besides introducing angular interactions, we also dynamically introduce dihedral interactions. A dihedral interaction involves four beads connected by three bonds, which defines a particular bond pattern, where the bonds can either be a hybridization bond, a 3'-5' backbone bond, or a 5'-3' backbone bond. Three bond patterns are possible. The bond pattern corresponding to red dihedrals in Fig. 2c, is characterized by $U(\Theta; \Theta_0 = 0, U_{\min,d})$ which favours a planar (cis) conformation. The bond pattern corresponding to blue dihedrals is characterized by $U(\Theta; \Theta_0 = \pi, U_{\min,d}, a = 0)$ which favours parallel backbone (trans) conformation. The last dihedral pattern corresponding to green dihedrals is characterized by $U(\Theta; \Theta_0 = 0, U_{\min,d})$ which favours a parallel (cis) conformation. Note that without the directional backbone bonds, we would not be able to distinguish between these two latter dihedral patterns.

During a simulation, at each time we introduce a hybridization bond, we also introduce up to four angular interactions and up to eight dihedral interactions – less if the hybridization bond is at the end of a strand. Let Δ be the total decrease in

binding energy when two beads hybridize inside a chain. We assign one third of this energy to bond, angular, and dihedral interactions, respectively. Hence $U_{\min, \text{hyb}} = \Delta/3$, $U_{\min, \text{a}} = \Delta/12$, and $U_{\min, \text{d}} = \Delta/18$. This choice does not affect the static properties of the model, which are determined by the total energy associated with a conformation, however it does influence the dynamic properties. We define $\Delta = 10\epsilon$ as a reference binding energy. Since only the ratio Δ/T enters the partition function of the model, this effectively fixes the absolute melting temperature of the strands. From a separate set of simulations at varying strand length n and temperature, we have determined the absolute strand melting temperatures as $T_m(n=3) = 0.74\epsilon$, $T_m(n=5) = 0.99\epsilon$, $T_m(n=10) = 1.29\epsilon$, and $T_m(n=15) = 1.49\epsilon$, which assuming room temperature as a reference energy ϵ corresponds to a melting temperature interval of -72 to 145 degrees for this range of strand lengths.

Fig. 1 shows the AND gate design that we are simulating. It consists of two toeholds of identical length t and two adjacent domains of length l . Note that we do not presently worry about garbage collecting the blocking strand after it has been displaced (Cardelli 2011). We have performed simulations of $(t, l) = (3, 10), (3, 12), (5, 10), (7, 8), (7, 10)$, and $(7, 14)$. Hence we can make comparisons varying toehold length for fixed total strand length ($n = 15$), varying the length of the adjacent domain for fixed toehold ($t = 7$), and varying the length of the toehold for fixed length of the adjacent domains ($l = 10$), respectively. To simulate the AND gate, we study a single strand of all the species in a simulation box of size $L = 40\sigma$. We insert the strands as straight conformations with a random position and orientation. Initially the blocking strand and the output signal strand are hybridized to the template molecule. We repeat each simulation at least ten times and in most cases twenty times starting from statistically independent initial states to obtain statistics on the observed hybridization kinetics. To estimate gate fidelity, we have also performed simulations where only one or none of the input signal strands are present. During a simulation, information is stored when a bond is created or removed between pairs of beads. Hence we know the entire hybridization bonding dynamics with Δt time resolution.

We can relate the simulation units to experimental units as follows. Identifying the bead-to-bead distance with the DNA rise distance $\sigma = 0.33\text{nm}$ maps to a strand concentration of $\approx 1\text{mM}$. This is quite high, but allows us to observe more strand collisions and hence to better characterize displacement kinetics. At lower concentrations most of the simulation time would be spent on diffusion of isolated strands, which is not of interest. The diffusion coefficient of a DNA model strand is $D(n) = k_B T \Gamma / (mn)$ where n is the total number of beads in a molecule. All simulations are run with $T = 1\epsilon$. This can be equated with the DNA diffusion coefficient of a particular experimental conditions to obtain a time mapping. Extrapolating the data in Ref. (Tinlan et al 1997) yields $\tau_L \approx 1.6 \times 10^{-12} \text{s}$ for $n = 20$. For the simulation of the AND gate we integrate the dynamics for 10^8 steps. This corresponds to approximately a microsecond of real time dynamics and such a simulation runs in approximately half a day on a powerful PC. Hence the run time per particle per step is approximately $1 \times 10^{-5} \text{s}$.

3 Results and discussion

Fig. 3 shows simulations of the strand displacement process of the AND gate (c.f. Fig. 1) using our Dynamic Bonded DNA model. As desired, the gate releases the AND signal (red) after binding both input strands (blue and green). Fig. 3 illustrates the dynamic

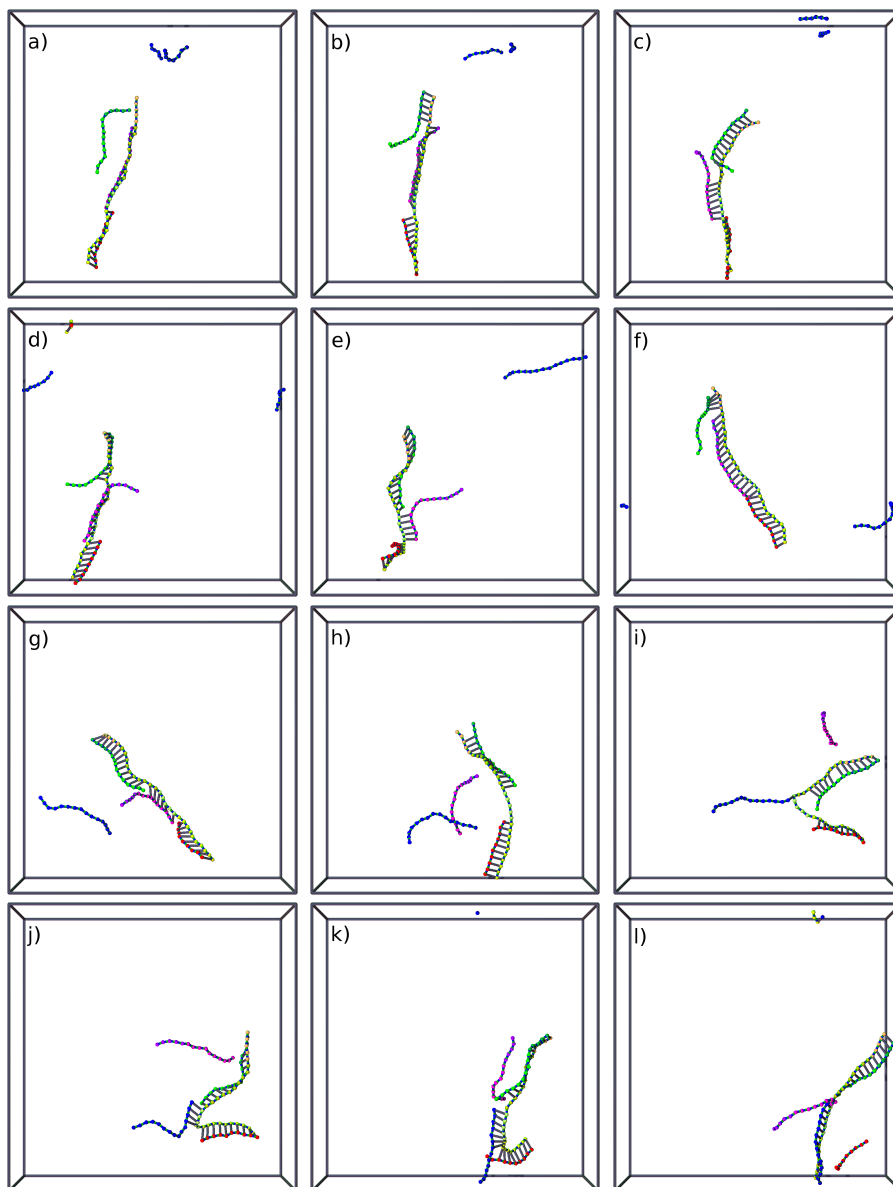


Fig. 3 Snapshots of strand displacement dynamics from a simulation with $(t, l) = (5, 10)$. The colours of the strands match Fig. 1. a) signal strand 1 (green) is close to toehold 1. b) hybridization of signal strand 1 and the blocking strand (magenta), c-g) diffusion of the branch point between the signal strand 1 and the blocking strand (magenta), h) the blocking strand finally displaced and the second toehold exposed, i) signal strand 2 (blue) is close to toehold 2, j) hybridization of signal strand 2, k-l) displacement and release of the output strand (red). The individual snapshots (a-l) are taken at times 8305, 8330, 8355, 8525, 8675, 9090, 9280, 9280, 12985, 13010, 13040, 13170. Note that we use periodic boundary conditions, hence strands leaving one side of the box enter the box on the opposite side. The simulations these snapshots are obtained from correspond to the simulation shown in row 7 in the top graph in Fig. 4.

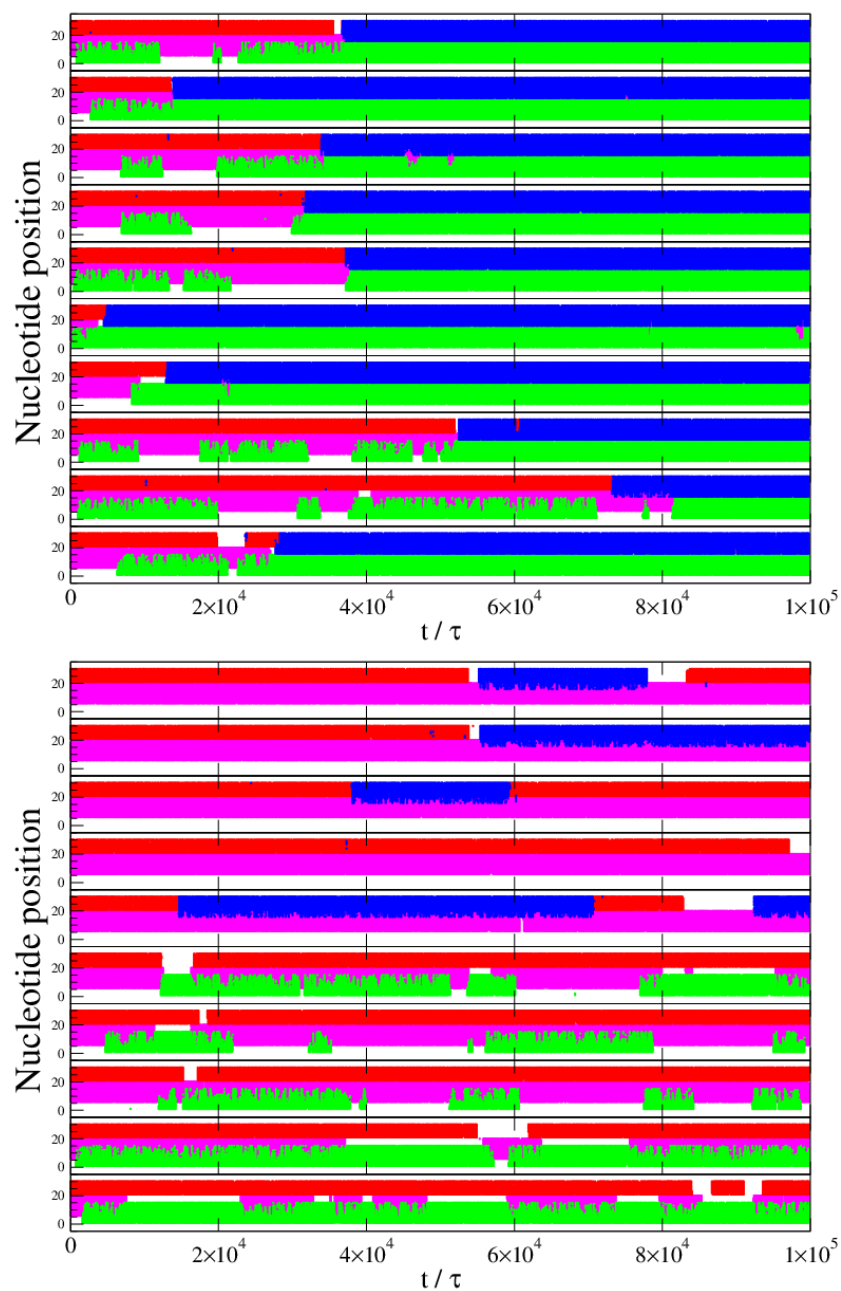


Fig. 4 Strand displacement dynamics for statistically independent simulations with $(t, l) = (5, 10)$ where both the signal strands (green and blue) are present (ten rows in the upper graph), and where only the second or the first signal strand (blue or green) is present (top five and bottom five rows in the lower graph, respectively). The hybridization state of each nucleotide along the template is shown colour coded along the y axis: blocking strand (magenta), first signal strand (green), second signal strand (blue), and the output strand (red).

nature of the strand displacement process as required by a single AND computation. Throughout the paper we will refer to the strands by the colour they have in Fig. 1. This colour coding is also used in the plots when referring to single strands. Fig. 3a-h shows how the green signal strand hybridizes with the template, and how the branch point between the green signal strand and the magenta blocking strands diffuses forwards and backwards until it finally displaces the magenta blocking strand. In the final steps (i-l), the blue signal strand hybridizes with toehold 2 and displaces the red output strand. This completes the strand displacement transitions constituting the AND computation. From the simulations in Fig. 3, we can also measure the durations of the transitions involved in the gate computation. The total transition time (a-l) of the AND gate is 4865τ from the initial binding of the green signal strand, subsequent binding of the blue signal strand until the final displacement of the red output strand. Whereas the first displacement transition (a-h) takes 975τ , the final displacement transition (i-l) takes just 185τ . In order to understand this kinetics, we must understand the physical dynamics of the AND gate in more detail.

In the first displacement transition (a-h), the initial (a) and final (h) states have essentially the same energy since the two toeholds have the same length. As a result the displacement process is completely reversible. We observe that the branching point between the two strands can diffuse backwards and forwards since when one of the strands is completely hybridized with the template, the other strand is still hybridized with a toehold. This competition for the domain first stops when one of the two strands is released from its toehold due to thermal melting. It is worth noting that a strand that is thermally irreversibly bound to a template can nevertheless be displaced by another strand with a longer complementary sequence. In the final displacement process (i-l), we observe the blue signal strand displacing the red output strand. This process is asymmetric since the red strand is only hybridized to the domain adjacent to toehold 2 and does not have a third toehold to hold on to. Hence when the blue signal strand has completely hybridized to the template, the red strand is released. This is the state with the minimum energy, since the system has decreased its total energy by the binding energy of toehold 1.

Fig. 4 shows 20 instances of the strand displacement dynamics of the operation of the AND gate. Note that the hybridization state is only shown for every $100\tau = 10^5\Delta t$, hence the plot only shows the most long-lived transitions. The upper graph shows the operation of the gate when both signal strands are present, whereas the bottom graph shows the gate operation when only the blue or the green signal strands are present (corresponding to the 11, 01, and 10 logic states of the gate respectively). We observe that the red output signal is irreversibly released in all simulations where both input strands are present. The computation is energetically downhill and driven by the binding energy of the first toehold with the green input strand. The lower graph in Fig. 4 shows the operation of the gate when only one of the two input strands is present. In the case where only the green strand is present, we see that it readily hybridizes with the template and competes with the magenta strand. In the case where only the blue strand is present, we see transitions where the blue strand hybridizes with the template and erroneously displaces the red signal strand. Both in simulations with one or both signal strands present, we observe transitions where the red output strand is erroneously released due to thermal melting of domain. When the blue strand is present we see that it displaces the red strand even though the second toehold is blocked by the magenta strand. We also observe that the red signal strand is eventually released in all simulations where both input strands are present. The red signal strand

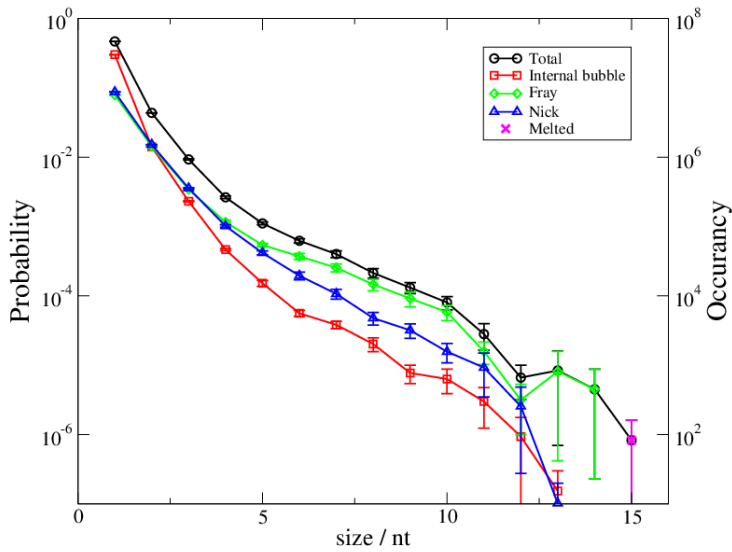


Fig. 5 Size probability distribution of all defect types (black circles), and the contributions from internal bubbles (red boxes), frays (green diamonds), nicks (blue triangles) for a template of length ($n = 30$) and two strands of length ($n = 15$) in a simulation of temperature $T = 1\epsilon$.

remains hybridized in most of the simulations where only the green input strand is present. However, we observe that the red signal strand is released quite often when then the blue input strand is present. Below we will quantify the gate fidelity for all the simulations and discuss this further.

We can also confirm that the dynamics we observed in the snapshots in Fig. 3 is indeed representative for the general strand displacement dynamics of the AND gate. Fig. 4 shows that there is strong competition between the green signal strand and the magenta blocking strand for hybridization with the domain 1, and the branching point can diffuse on the domain for an extended period of time. The diffusion process stops when one of the two strands leaves its toehold due to thermal melting. Hence the duration of these processes should depend exponentially on the length of the toehold. We also observe that the displacement of the red strand by the blue signal strand is a much faster process, which can hardly be resolved in the figure.

Fig. 4 shows that the simple “textbook” pathway illustrated in Fig. 1 is by no means the only or even the most likely pathway from the initial to the final state of the AND gate. Although the final state is reached with good fidelity, there are many possible pathways that the system can follow to reach this state. These simulations illustrate the less than ideal behaviour of strand displacement gates that will occur when they are implemented in real chemistry. At non-zero temperature a DNA strand will always have transient stretches or bubbles of thermally broken hybridization bonds as these contribute configurational entropy, and hence reduce the free energy. (Blossey and Carlon 2003) In the case where a such a bubble is at the free end of the template it is denoted a fray, whereas we denote it a nick when the bubble originates at the interface between two strands hybridized to the template. These defects can transiently

expose long stretches of nucleotides where a free complementary strand can bind and transiently or permanently displace the original strand.

To characterize the occurrence of bubbles, frays, and nicks in our DNA AND gate, we have performed simulations of the final state corresponding to Fig. 1f without the displaced magenta and red strands being present in solution. These simulations have been run up to $t = 10^5\tau$ as the other simulations. At each time step, we analyse the blue and green strand conformations for internal bubbles, frays at the ends of the template, or nicks at the interface between the green and blue strands. The corresponding probability distributions are shown in 5. We observe an approximately exponential decrease in defect probability as the defect length increases. In 50% of the sampled conformations a single hybridization bond is found to be broken, which is most likely an internal bubble. Already defects of three nucleotides and longer are significantly more likely to be frays or nicks, and the largest defects are predominantly frays. This is expected since nicks and in particular frays have less stabilizing angular and dihedral interactions compared to a nucleotide inside a double strand. While the probability of these large defects is small, the simulation is long enough that their occurrence is significant. If such a defect occurs while a longer complementary strand is within hybridization distance of the template, then these thermally induced defects will cause undesired strand displacement transitions.

To analyse the strand displacement dynamics in more detail, we measure the duration of each hybridization \rightarrow release transition of each single strand. This is the time from when the first hybridization bond between a particular strand and the template is created until the last hybridization bond is broken and the strand is released. Note that these do not need to coincide with the first or last nucleotides of the respective domains. E.g., for the green strand transition, pathways such as $b \rightarrow a$, $b \rightarrow c \rightarrow b \rightarrow a$, and $b \rightarrow c \rightarrow d \rightarrow c \rightarrow b \rightarrow a$ in Fig. 1 all contribute to the hybridization \rightarrow release transitions. The large number of possible transition pathways already suggests that we can expect a very broad time distribution of these transitions. Note that the first release of the magenta and red strands is not sampled, since they are already hybridized with the template when the simulation starts. Equally, incomplete transitions at the end of the simulation are also discarded.

In the following plots, we show the cumulative distributions $C(t) = \int_0^t P(t') dt'$ rather than the probability density $P(t)$. Our measured probability densities are of the form $P(t) = N^{-1} \sum_i^N \delta(t - t_i)$ where δ is the Dirac delta function and t_i is the duration of hybridization \rightarrow release event i we obtained from simulation. To represent this distribution as a continuous distribution would require binning, which could potentially introduce artefacts in the representation. Instead, the cumulative distribution is increased by N^{-1} every time an event occurs. In this representation a high density of events i.e. a peak in a continuous probability distribution produces a high slope in the cumulative distribution, whereas a flat plateau indicates zero probability density of events. Below by peaks we denote regions of high slope in the cumulative distributions. The median transition time $\langle t \rangle$ is trivially read off at $C(\langle t \rangle) = 0.5$.

Ideally, if the gate follows the pathway indicated in Fig. 1, we would not observe a single hybridization \rightarrow release transition. The blue and green signal strands would bind irreversibly and never be released. The magenta blocking strand and the red output strand would be released only once, but they would never rehybridize with the template. Fig. 6 shows the cumulative distributions of these transitions for each of the four strands constituting the operation of the AND gate when both signal strands are present.

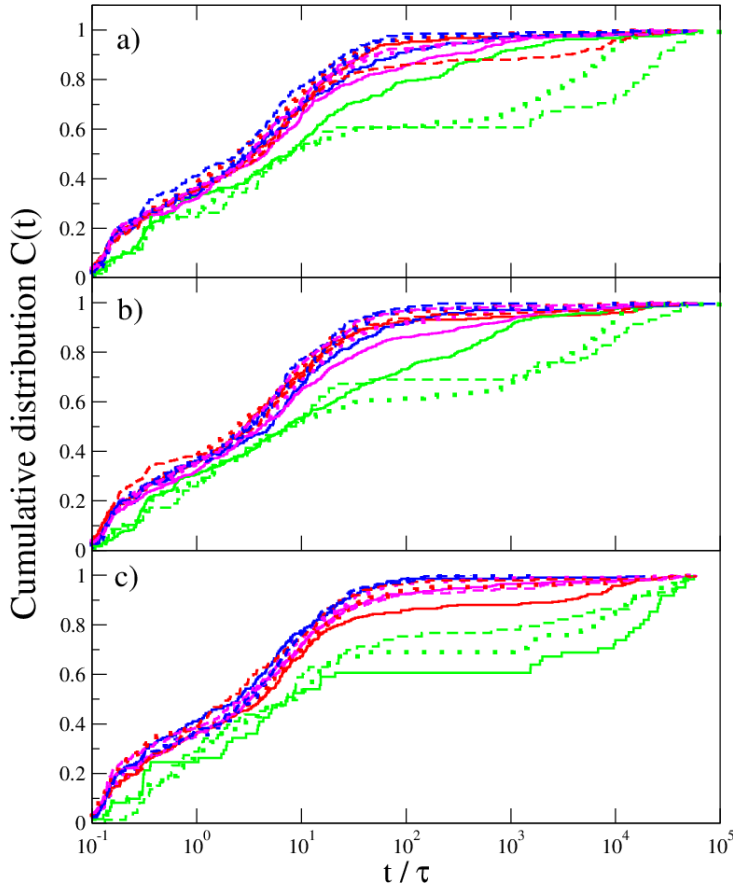


Fig. 6 Cumulative probability distributions for the duration of hybridization→release transitions of each strand for simulations with a) constant strand length $(t, l) = (3, 12), (5, 10), (7, 8)$, b) varying toehold size $(t, l) = (3, 10), (5, 10), (7, 10)$, and c) varying domain size $(t, l) = (7, 8), (7, 10), (7, 12)$ using solid, dotted, and dashed lines, respectively, for the three systems. The colours denote the strand type: signal strand 1 (green), signal strand 2 (blue), blocking strand (magenta), and output strand (red).

Clearly, we see a large number of transitions occurring for all the strands involved with the gate computation. Furthermore, we observe an extremely wide distribution of transition times covering at least six orders of magnitude in time. Since the simulations are run up to $10^5\tau$, this imposes an upper limit on the observable transitions. It is likely that a fraction of transitions would occur on even longer time scales.

Overall, the distributions shown in the figure are very similar. Most of the fast transitions of the blue signal strand and the magenta blocking strand occur on time scales of $10^{-1} \dots 10^2\tau$, although about 10% of the transitions are in the long tail of the distribution. We also observe a large number of slow transitions for the green signal strand that occurs on time scales of $10^{-1} \dots 10^5\tau$. For most of the simulations, except for the one with the shortest domain length, we also observe fast transitions for the red output strand. Note that only slow transitions with $t \gg 10^2\tau$ are visible in

Fig. 4 For the fast transitions, the distributions are quite similar, and they correspond to a distribution with two peaks one centered around $t \sim 10^{-1}$ and $10^1\tau$. The first peak probably corresponds to binding events where one or a few hybridization bonds are made to nucleotides exposed within defects, but where the invading strand is rapidly displaced. The second peak probably corresponds to binding events where most of the strand hybridizes with the template, but is subsequently displaced by another strand. Alternatively, this can be interpreted in light of the free energy of the transition. The hybridization binding energy favours the double stranded state, however, the entropy favours having a pair of single strands, since this maximise the number of possible conformations of the system. The double peak is suggestive of an free energy barrier of hybridization, where the reduction in free energy due to a few initial hybridization bonds have not yet been balanced by the loss in entropy due to the loss of possible conformations. For the green strand, a third broad peak appears at very large time scales, and 20 – 40% of the transitions are long-lived. These are the reversible strand displacements where the green signal strand and the magenta blocking strands are competing for the template, and where both are hybridized to their respective toeholds. With this in mind, one would naively expect the same transition time distribution for the magenta blocking strand and the green signal strand, since their displacement process is energetically reversible. However, the magenta blocking strand is also competing for toehold 2 with the blue strand. When the blue strand hybridizes with toehold 2 and displaces the red output strand, this is the state with the minimal energy. Hence the magenta blocking strand is prevented from rehybridizing with toehold 2 and displacing the green signal strand. This explains why the transitions of the magenta blocking strand take about the same time as the green signal strand but are much rarer.

Looking at the kinetic dependence on the lengths of the toeholds and domains, we see a strong influence on the transitions of the green strand, but relatively little influence on the transitions of the other strands as long as the toehold is short compared to the adjacent domain. We observe a dramatic slowing down of the transitions of the green signal strand as the length of toehold 1 is increased, whereas the duration of the transition remains around $10^4\tau$ when the toehold length is kept fixed. If we want to minimise the duration of the green strand displacement transitions, we should instead increase the domain length compared to the toehold length as shown by the two simulations with $(t, l) = (3, 12)$ and $(3, 10)$.

Just as we can measure the durations of all the hybridization \rightarrow release transitions, we can also measure all the release \rightarrow hybridization transitions. Whereas the former characterize the cooperative and competitive kinetics of the hybridization processes, the latter characterize bulk diffusion between these binding events. As a result we expect these to depend strongly on the concentration, whereas the hybridization \rightarrow release transitions are not expected to be strongly dependent on concentration. Fig. 7 shows the distribution of the release \rightarrow hybridization transition times. We see relatively little structure in these cumulative distributions: they are approximately linear over three to four orders of magnitude with a peak around $10^4\tau$. The approximately linear relation between cumulative probability and the logarithm of time seen in the figure corresponds to a transition probability distribution $P(t) \propto t^{-1}$ for $0.1 < t < 10^3\tau$. The peak is most likely an artefact due to the periodic boundary conditions that we apply in the simulations. When a strand is released it will diffuse in free space and return to the template. However, it can also return to any of the periodic images of the template. These periodic images define a cubic lattice with spacing $L = 40\sigma$. If the free

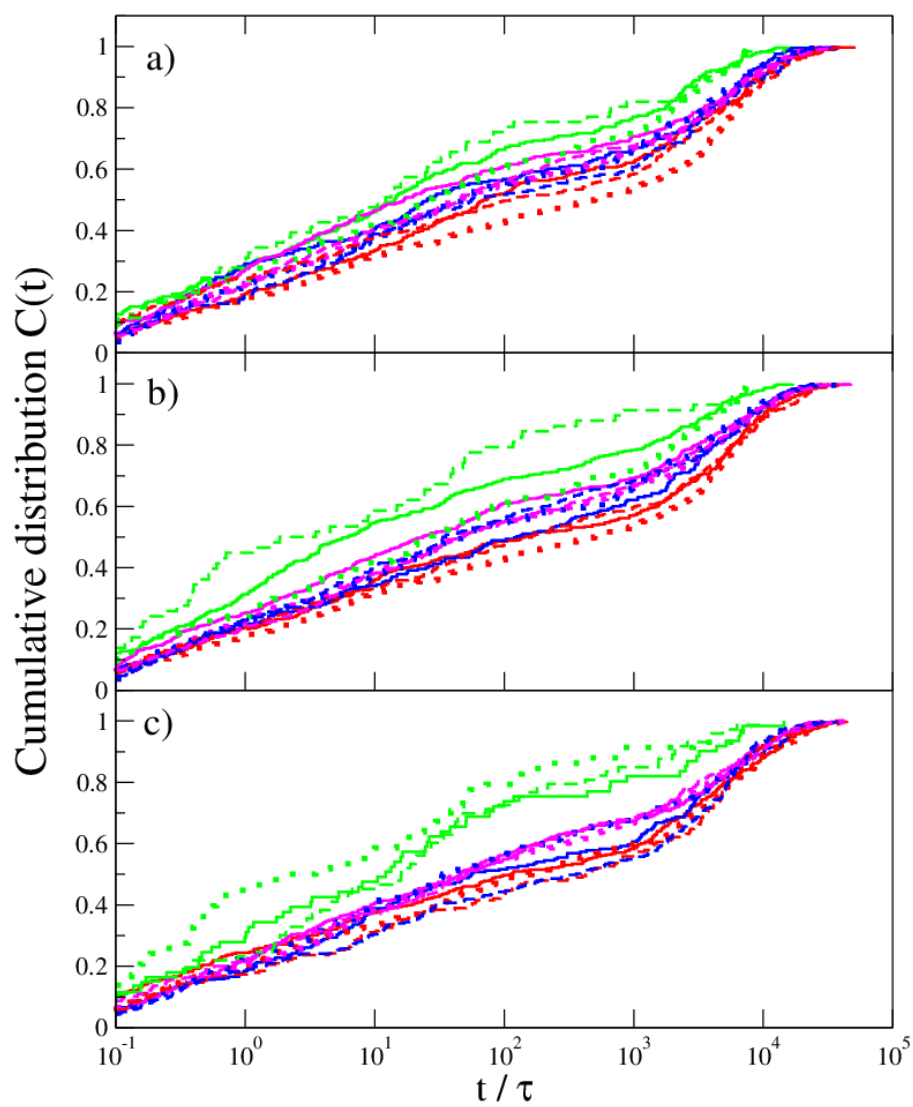


Fig. 7 Cumulative probability distributions for the durations of release \rightarrow hybridization transitions of each strand for simulations with a) constant strand length $(t, l) = (3, 12), (5, 10), (7, 8)$, b) varying toehold size $(t, l) = (3, 10), (5, 10), (7, 10)$, and c) varying domain size $(t, l) = (7, 8), (7, 10), (7, 12)$ using solid, dotted, and dashed lines, respectively, for the three systems. The colours denote the strand type: signal strand 1 (green), signal strand 2 (blue), blocking strand (magenta), and output strand (red).

strands could hybridize with each other or with garbage collecting DNA templates, we would expect to see more structure in these transitions. Surprisingly the green strand exhibits faster release \rightarrow hybridization transitions than the magenta strand. This indicates that the binding kinetics of the first and second toehold are in fact different, which could be due to the presence of the blue strand, or the fact that toeholds at the end and internally in a strand are not equally accessible.

Of key interest is the average time of the total AND computation and its three constituting transitions. Therefore, we measure the time between the first hybridization of the green signal until the final release of the magenta blocking strand (Fig. 1 b to c). Similarly, we measure the time between the release of the magenta blocking strand and the first hybridization of the blue input strand, as well as the time between the first hybridization of the blue strand and the final release of the red signal strand. In light of the complex sequence of transition events that we observe in Fig. 4, a non-trivial question is how to define the pattern of transition events that most accurately characterize the duration of the full computation transition. We choose to start (or reset) the clock when the green input strand hybridizes with the template in the input state (Fig. 1a), i.e. where the magenta blocking strand and the red output strand are hybridized with the template. The first milestone is the release event of the magenta blocking strand. The second milestone is the hybridization of the blue input signal. We stop the clock the first time the red output strand is released (e.g. Fig. 1f). Note that this event pattern specifies a certain causal ordering of milestones, but it does not define a unique sequence of consecutive events, since we allow hybridization \rightarrow release events between the specified milestones. Furthermore, in the final state we do not require the magenta blocking strand to be in solution, nor that the green and blue input strands remain hybridized with the template. This definition is a compromise between an ideal, maximally restrictive definition and a more pragmatic definition. The latter definition allows to analyse our realistic simulation data in a meaningful way. It is worth noting that we have not observed a single AND computation characterized by the maximally restrictive definition.

Fig. 8 shows the cumulative distributions of the two strand displacement transition times, the binding transition time and the total gate transition time. The fastest strand displacement process is the final displacement of the red output strand by the blue signal strand. The third transition takes $\approx 10^2\tau$ and is energetically downhill when the second toehold is exposed. We observe that increasing the domain length leads to somewhat slower displacement times, while varying the toehold length has little influence on the displacement speed. This is consistent with the increased time it takes the branching point to diffuse across a longer domain after the blue input strand has hybridised with the second toehold. The second transition is the binding of the blue input strand after the magenta blocking strand has been displaced. We observe that this requires $\approx 10^3\tau$ and appears to be largely independent of the length of the toehold and adjacent domain. This is expected since this is only determined by the time it takes the blue strand to diffuse and bind to the template when the second toehold is exposed. The first transition is the displacement of the magenta blocking strand by the green signal strand. This transition takes significantly longer time than the first transition but is comparable with the duration of the second transition. We observe a very strong dependence on toehold length and a much weaker dependence on domain length. Increasing the toehold length from three to seven increases the duration of the transition by more than an order of magnitude. This is consistent with the exponential slowing down of the displacement kinetics when the toehold is elongated (Yurke and

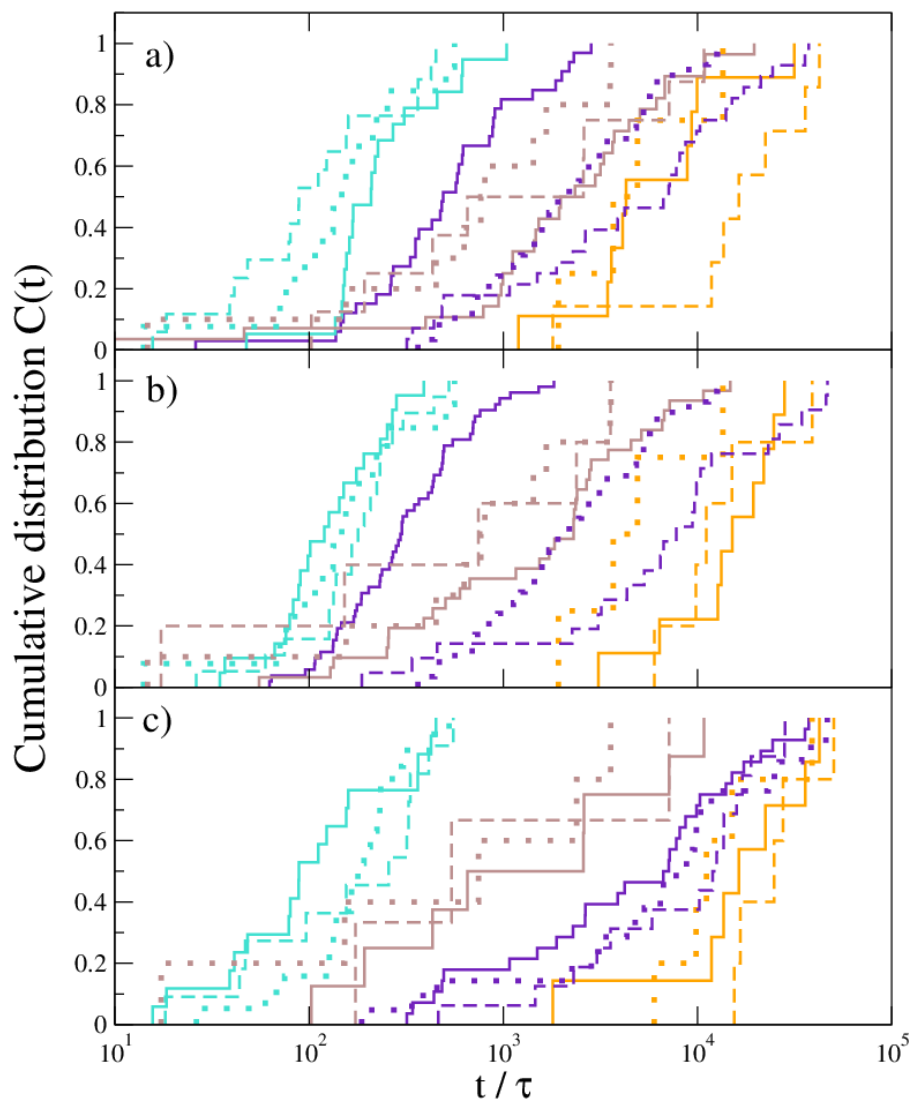


Fig. 8 Cumulative probability distributions for the duration of the gate operation and its three constituting displacement transitions for simulations with a) constant strand length $(t, l) = (3, 12), (5, 10), (7, 8)$, b) varying toehold size $(t, l) = (3, 10), (5, 10), (7, 10)$, and c) varying domain size $(t, l) = (7, 8), (7, 10), (7, 12)$ using solid, dotted, and dashed lines, respectively. The colours denote the type of transition: hybridization of the green signal strand \rightarrow release of the magenta blocking strand (indigo), release of the magenta blocking strand \rightarrow hybridization of the blue signal strand (light brown), hybridization of the blue signal strand \rightarrow release of the red output strand (turquoise), and total AND gate computation transition time (orange).

Mills 2003): the magenta strand is most likely to thermally melt of the second toehold when the green input strand is completely hybridized with the template. The energetic barrier of thermal melting is exponential in the length of the double stranded domain. The weaker dependence on domain length that we observe is again due to the diffusion of the branching point when the magenta blocking strand and the green input strand are competing for the template. Finally, we observe that the total transition time is approximately $2 \times 10^4 \tau$. Remarkably, the total gate computation transition time appears to be rather insensitive to the size of the toeholds and adjacent domains. The distribution of gate operation times can be approximated by the convolution of the three distributions associated with the three transitions required for the gate operation. This suggests that the exponential toehold dependence of the first transition is in part countered by the toehold size independent second and third transitions. With the few data points we have for the total gate operation time, it is difficult to extract any general trends from our data.

We can characterize the gate fidelity as the probability that the red output signal has been released after the gate transition. In the ideal case, this probability would reproduce the logic table of an AND gate. We estimate the fidelity by sampling conformations for $t \geq 8 \times 10^4$, where the AND gate transition should have taken place. We have performed at least ten statistical independent simulations of each AND gate which allows us to estimate the accuracy of the fidelity. Tab. 3 shows the fidelity of the AND gate for various simulated domain lengths. We observe excellent fidelity for all logic states except the 01 input state. This shows that gate operation has completed in the time window we use to estimate the fidelity.

In the 01 input state, only the blue input strand is present. Its low fidelity could be attributed either to thermal melting of the red output strand or displacement of the red output strand by the invading blue input strand due to transient defects. If thermal melting was the dominant cause, we would expect the fidelity of the 10 and 00 logic states to be affected too. Hence we attribute the observed lack of fidelity to defect induced strand displacement, where a transient bubble allows the blue input strand to displace the red output signal. The binding energy of this faulty state corresponds to that of the correct state, and hence they appear equally likely (disregarding entropic contributions to the free energy). This is in agreement with the fidelity ≈ 0.5 that we observe in all the simulations. Both the correct and the faulty states are long lived, since they require the fortuitous opening of a bubble while the competing strand is within hybridization distance. This explains why the accuracy for the 01 logic state is much less than the other states, because different simulations essentially sample only the correct or the faulty state. In experiments, this might be suppressed by decreasing the concentration of strands, however to study this further is outside the scope of the present paper.

4 Conclusions

We have studied strand displacement dynamics, in particular kinetics and fidelity of an AND gate implemented using DNA strand displacement dynamics, which form the basis of state-of-the-art DNA computing approaches. The ideal causal strand displacement dynamics shown in the textbooks is one where the first signal strand displaces a blocking strand to expose a second toehold, which is hybridized with a second signal strand to finally release the output strand indicating the true state of

$t \setminus l$	8		10		12	
3			11	0.97 ± 0.02	11	0.90 ± 0.06
			10	0.00 ± 0.00	10	0.00 ± 0.00
			01	0.60 ± 0.11	01	0.37 ± 0.15
			00	0.03 ± 0.02	00	0.00 ± 0.00
5			11	0.95 ± 0.04		
			10	0.05 ± 0.03		
			01	0.41 ± 0.14		
			00	0.01 ± 0.01		
7	11	0.90 ± 0.06	11	0.95 ± 0.05		
	10	0.01 ± 0.01	10	0.02 ± 0.01		
	01	0.65 ± 0.14	01	0.58 ± 0.15		
	00	0.06 ± 0.03	00	0.00 ± 0.00		

Table 1 Fidelity of AND gates for the simulated choices of toehold t and adjacent l domain sizes for the four logic possibilities where both input strands are present (denoted 11), where only the green input strand is present (denoted 10), where only the blue input strand is present (denoted 01), and finally where none of the input strands are present (denoted 00). The error estimate is obtained from the analysis of at least ten statistically independent simulations.

the DNA AND gate. Furthermore, for the ideal AND gate, no signal is released if none or just one of the two signal strands are present. However, chemical implementations of strand displacement gates have to content with non-ideal behaviour that originates from thermal effects, which changes the textbook picture.

We have implemented a DNA AND gate within the framework of molecular dynamics simulations utilizing a coarse-grained dynamic bonded molecular model of DNA molecules that we have recently developed. We study an AND gate design where a template strand has a first toehold, a first domain, a second toehold, and a second domain. Initially the first toehold is exposed, while a blocking strands is hybridized to the first domain and the second toehold. The output strand is hybridized with the second domain only. The first input signal hybridizes with the first toehold and partially displaces the blocking strand. When the blocking strand dehybridises, the second toehold is exposed. The second input strand can hybridise with the second toehold and displace the output signal, hence completing the operation of the gate. We have performed extensive simulations of this design to study gate operation for toehold lengths from 3 to 7 and domains 8 to 12 nucleotides long for systems of fixed temperature. Mapping these length ranges to melting temperatures of DNA strands produces a range in excess of $200K$ from the shortest toehold to the longest strand. Each simulation was performed with at least ten statistical independent initial states.

In our analysis of the simulation results we observe a complex sequence of dynamic transitions, where strands are released and rehybridize numerous times; we see release of the output signal before either of the two input strands are bound to the gate; and we even observe the release of the output signal in the absence of input strands. All these effects are due to thermal melting and bubbles and are expected to occur in a chemical implementations of strand displacement gates. We have characterized the type of defects present in a DNA AND gate in the final state. This shows that transient internal bubbles occurs with a high frequency, while defects longer than 3 nucleotides are prevalently located at the end of the template or at nicks between hybridized strands.

We have characterised the gate kinetics by analysing the distribution of times it takes from hybridization to release of a strand, as well as the times required from the release to rehybridization of a strand. These give insights into the binding kinetics and bulk diffusion, respectively.

We have also analysed the total gate operation time as well as the three transitions that it is based on: hybridization of the first input signal, release of the blocking strand, subsequent hybridization of the second input strand, and finally release of the output signal. We see that the first displacement transition is exponentially dependent on the toehold size, while the second and third transitions are essentially independent of the toehold size. We also see a weaker dependence on domain length of the displacement processes. Remarkably the total operation time appears to be largely independent of both the toehold and adjacent domain size at least within the range of lengths studied in the present paper. This latter time distribution is approximately the convolution of the time distributions associated with the three transitions, and the second and third transitions effectively cancel the exponential toehold dependence of the first transition.

From the simulation results we can evaluate the fidelity of the gate operation. Ideally, the probability of the output strand being released after the gate has finished its operation should correspond to the logic table of an AND operation. We observe excellent gate fidelity except for the input state where only the second input signal is present, which has quite poor fidelity. In this case, we observe that bubbles create transient toeholds that allow the second strand to displace the output signal, and compete with the blocking strand for the second toehold. This faulty state has the same number of hybridization bonds and appears to be as favourable as the correct state where the output signal remains hybridized with the template.

In conclusion, we have shown that computer simulations of the kind presented expose the detailed molecular mechanisms behind non-ideality, and in particular how non-ideality influences kinetics and fidelity of DNA strand displacement computation. The presented simulation studies also illuminate how to realise optimal implementations of logic gates in DNA strand displacement operations, in terms of balancing high fidelity and fast computation transition times. We could also use simulations such as these as a starting point for developing and testing first principle statistical mechanical theories predicting the physical-chemical behaviour of DNA strand displacement systems.

5 Acknowledgements

The research leading to these results was sponsored in part by the European Community's Seventh Framework Programme under grant agreement no 249032 (MATCHIT), in part by the Danish National Research Foundation and in part by the University of Southern Denmark. The work was conducted at the Center for Fundamental Living Technology (FLinT). We are grateful to Pierre-Alain Monnard for critical advice concerning DNA properties.

References

- Adleman LM (1994) Molecular computation of solutions to combinatorial problem. *Science* 266:1021
- Altan-Bonnet G, Libchaber A, Krichevsky O (2003) Bubble dynamics in double-stranded dna. *Phys Rev Lett* 90:138,101

- Amos M, Dittrich P, McCaskill J, Rasmussen S (2011) Biological and chemical information technologies. *Proc Comp Sci* 7:56
- Blossey R, Carlon E (2003) Reparametrizing the loop entropy weights: Effect on dna melting curves. *Phys Rev E* 68:061,911, DOI 10.1103/PhysRevE.68.061911, URL <http://link.aps.org/doi/10.1103/PhysRevE.68.061911>
- Brooks BR, Brooks CL III, Mackerell AD Jr, Nilsson L, Petrella RJ, Roux B, Won Y, Archontis G, Bartels C, Boresch S, Caffisch A, Caves L, Cui Q, Dinner AR, Feig M, Fischer S, Gao J, Hodoseck M, Im W, Kuczera K, Lazaridis T, Ma J, Ovchinnikov V, Paci E, Pastor RW, Post CB, Pu JZ, Schaefer M, Tidor B, Venable RM, Woodcock HL, Wu X, Yang W, York DM, Karplus M (2009) CHARMM: The Biomolecular Simulation Program. *J Comput Phys* 30:1545
- Cardelli L (2011) Strand algebras for DNA computing. *Nat Comput* 10:407
- Case DA, Darden TA, Cheatham III TE, Simmerling CL, Wang J, Duke RE, Luo R, Walker RC, Zhang W, Merz KM, et al (2010) AMBER 11. University of California, San Francisco
- Cheatham III TE, Young MA (2000) Molecular dynamics simulation of nucleic acids: Successes, limitations, and promise. *Biopolymers* 56:232
- Gil B, Hadorn M, Shabi U, Shapiro E, Hanczyc MM (2013) Unpublished
- Hadorn M, Eggenberger Hotz P (2010) DNA-mediated self-assembly of artificial vesicles. *PLoS One* 5:e9886
- Hadorn M, Boenzi E, Sørensen K, Fellermann H, Eggenberger Hotz P, Hanczyc MM (2012) Specific and reversible dna-directed self-assembly of oil-in-water emulsion droplets. *PNAS*
- Hsu CW, Sciortino F, Starr FW (2010) Theoretical description of a DNA-linked nanoparticle self-assembly. *Phys Rev Lett* 105:55,502
- Jost D, Everaers R (2007) A unified description of poly- and oligonucleotide DNA melting: nearest-neighbor, Poland-Sheraga and lattice models. *Phys Rev E* 75:041,918
- Jost D, Everaers R (2009) A unified Poland-Scheraga model of oligo- and polynucleotide DNA melting: Salt effects and predictive power. *Biophys J* 96:1056
- Kramers HA (1940) Brownian motion in a field of force and the diffusion model of chemical reactions. *Physica* 7:284
- Lakin MR, Youssef S, Cardelli L, Phillips A (2012) Abstractions for DNA circuit design. *J R Soc Interface* 9:470
- Lane MJ, Paner T, Kashin I, Faldasz BD, Li B, Gallo FJ, Benight AS (1997) The thermodynamic advantage of DNA oligonucleotide stacking hybridization reactions: energetics of a DNA nick. *Nucl Acids Res* 25:611
- Langowski J (2006) Polymer chain models of DNA and chromatin. *Eur Phys J E Soft Matter* 19:241
- MacKerell Jr AD, Banavali N, Foloppe N (2000) Development and current status of the CHARMM force field for nucleic acids. *Biopolymers* 56:257
- Martinez-Veracochea FJ, Mladek BM, Tkachenko AV, Frenkel D (2011) Design rule for colloidal crystals of DNA-functionalized particles. *Phys Rev Lett* 107:045,902
- Ouldridge TE, Louis AA, Doye JPK (2010) DNA nanotweezers studied with a coarse-grained model of DNA. *Phys Rev Lett* 104:178,101
- Ouldridge TE, Louis AA, Doye JPK (2011) Structural, mechanical, and thermodynamic properties of a coarse-grained DNA model. *J Chem Phys* 134:085,101
- de Pablo JJ (2011) Polymer simulations: From DNA to composites. *Annu Rev Phys Chem* 62:555
- Peyrard M, Cuesta-Lopez S, James G (2008) Modelling DNA at the mesoscale: a challenge for nonlinear science? *Nonlinearity* 21:T91
- Plimpton S (1995) Fast parallel algorithms for short-range molecular dynamics. *J Comp Phys* 117:1, URL <http://lammps.sandia.gov>
- Poland D, Scheraga HA (1966) Phase transitions in one dimension and the helix-coil transition in polyamino acids. *J Chem Phys* 45:1456
- Protozanova E, Yakovchuk P, Frank-Kamenetskii M (2004) Stacked - unstacked equilibrium at the nick site of DNA. *J Mol Bio* 342:775
- Qian L, Winfree E (2011) Scaling up digital circuit computation with DNA strand displacement cascades. *Science* 332:1196
- Sambriski EJ, Ortiz V, de Pablo JJ (2009a) Sequence effects in the melting and renaturation of short DNA oligonucleotides: structure and mechanistic pathways. *J Phys Condens Matter* 21:034,105

-
- Sambriski EJ, Schwartz DC, de Pablo JJ (2009b) A mesoscale model of DNA and its renaturation. *Biophys J* 96:1675
- SantaLucia JJ, Hicks D (2004) The thermodynamics of DNA structural motifs. *Annu Rev Biophys Biomol Struct* 33:415
- Savelyev A, Papoian GA (2010) Chemically accurate coarse graining of double-stranded DNA. *PNAS* 107:20,340
- Seelig G, Soloveichik D, Zhang DY, Winfree E (2006) Enzyme-free nucleic acid logic circuits. *Science* 314:1585
- Svaneborg C (2012) LAMMPS framework for dynamic bonding and an application modeling DNA. *Comp Phys Comm* 183:1793
- Tinlan B, Pluen A, Sturm J, Weill G (1997) Persistence length of single-stranded DNA. *Macromolecules* 30:5763
- Yurke B, Mills AP (2003) Using DNA to power nanostructures. *Genet Prog Evol Mach* 4:111
- Zhang DY, Winfree E (2009) Control of DNA strand displacement kinetics using toehold exchange. *J Am Chem Soc* 131:17,303